Chemical Science

ROYAL SOCIETY OF CHEMISTRY

EDGE ARTICLE

View Article Online
View Journal | View Issue

Cite this: *Chem. Sci.*, 2021, **12**, 7763

All publication charges for this article have been paid for by the Royal Society of Chemistry

Received 16th February 2021
Accepted 15th April 2021

DOI: 10.1039/d1sc00929j

rsc.li/chemical-science

Tumor chemical suffocation therapy by dual respiratory inhibitions†

Yingying Xu,[ab] Yuedong Guo,[a] Lei Chen,[c] Dalong Ni,[a] Ping Hu*[a] and Jianlin Shi*[ad]

The extraordinarily rapid growth of malignant tumors depends heavily on the glucose metabolism by the pathways of glycolysis and mitochondrial oxidative phosphorylation to generate adenosine 5′-triphosphate (ATP) for maintaining cell proliferation and tumor growth. This study reports a tumor chemical suffocation therapeutic strategy by concurrently suppressing both glycolysis and mitochondrial oxidative phosphorylation (OXPHOS) *via* the co-deliveries of EDTA and rotenone into a glutathione (GSH)-overexpressed tumor microenvironment. EDTA is to block the glycolytic pathway through inhibiting the activity of glycolytic enzymes *via* the chelation of magnesium ion, a co-worker of glycolytic enzymes, despite the presence of Ca^{2+}. Meanwhile rotenone is to inhibit the mitochondrial OXPHOS. This work provides a novel tumor suffocation strategy by the co-deliveries of glucose metabolism inhibitors, especially by de-functioning glycolytic enzymes *via* eliminating their co-worker magnesium.

Introduction

Cancer cells proliferate indefinitely and thus need much more energy than normal cells. Especially, glucose metabolism of cancer has attracted great attention since Otto Warburg observed that cancer cells rely primarily on aerobic glycolysis to produce adenosine 5′-triphosphate (ATP) for various cellular processes.[1,2] Glucose is the dominant source of energy in cancer cells through mitochondrial oxidative phosphorylation (OXPHOS), a normal aerobic respiration process, and glycolysis, a glucose metabolism mechanism under oxygen-deficient conditions. Therein, glycolysis usually works as the main mode to generate ATP to maintain exaggerated tumor growth. In detail, glycolytic process involves several kinases that contribute to energy generation, including hexokinase (HK), phosphofructokinase (PFK) and pyruvate kinase (PK), all of which are key kinases to regulate glucose phosphorylation and dephosphorylation.[3] These enzymes are the rate-limiting components for the glycolytic process and responsible for one-way reactions. A common but vitally important feature is that all the kinases should be activated to play their roles in glycolysis by Mg^{2+}, *i.e.*, the glycolytic process would not take place without Mg^{2+}.[4–6] Therefore, eliminating the intracellular Mg^{2+} could be probably an efficient strategy to inhibit cancer cell glycolysis, in addition to the effective aerobic respiration suppression.

Plenty of evidences have proved that rotenone plays direct inhibition roles in mitochondrial dysfunctions, such as interference to the electron transport chain, mitochondrial membrane potential loss and reducing ATP production.[7–9] Rotenone is therefore an effective inhibitor of mitochondrial respiratory chain complex I, blocking the electron transport during mitochondrial OXPHOS.[10] It is therefore indeed feasible to apply rotenone to suppress mitochondrial OXPHOS, however, tumor cells can still survive through glycolysis once mitochondrial OXPHOS has been inhibited.

As a common industrial agent known for complexing metal ions in water,[11] ethylenediaminetetraacetic acid (EDTA) shows a strong chelating capability with a number of metal ions, such as Mg^{2+} ($pK_a = 8.7$).[12] As far as we know, there have been no reports of using EDTA for inhibiting tumor glycolysis. Inspired by the finding about the indispensable role of Mg^{2+} in glycolysis, it can be reasoned that glycolysis may be blocked or even stopped *via* chelation-deprived magnesium ions by EDTA, thus inhibiting the activities of hexokinase, phosphofructokinase and pyruvate kinase. Therefore, we suppose that the simultaneous use of rotenone and EDTA may be an effective strategy to cut off tumor cell respiration comprehensively. Hereinto, it is necessary to design a competent delivery system to deliver the above molecules into tumor cells.

[a]*The State Key Laboratory of High Performance Ceramics and Superfine Microstructures, Shanghai Institute of Ceramics, Chinese Academy of Sciences, 1295 Ding-xi Road, Shanghai 200050, P. R. China*

[b]*School of Physical Science and Technology, ShanghaiTech University, 393 Middle Hua-xia Road, Shanghai 201210, P. R. China*

[c]*Department of Chemistry, Fudan University, 220 Han-dan Road, Shanghai 200433, P. R. China*

[d]*Innovative Center of Medicine, Shanghai Tenth People's Hospital, 38 Yun-xin Road, Shanghai 200435, P. R. China*

† Electronic supplementary information (ESI) available. See DOI: 10.1039/d1sc00929j

Researchers have been making significant progresses in cancer therapy by developing drug delivery systems employing various nano drug carriers, such as mesoporous silica nanoparticles (MSNs), layered double hydroxides (LDH), dendrimers and polymer micelles.[13–18] Therein, MSNs feature high drug loading ability, feasible chemical modification and good biosafety. Hence, MSNs were chosen as the delivery platform. Because of the significant difference in the GSH concentration between the extracellular (2–10 μM) and intracellular (2–20 mM) environment,[19–22] redox potential has become a typical stimulus of various responsive delivery systems. Moreover, the concentration of GSH in most tumor cells is at least four times than that in normal cells.[23] In order to minimize the damage to normal cells, a glutathione (GSH)-responsive shell could be modified on the outer surface of MSNs. In this article, we report a GSH-responsive nanoplatform, MSN/EDTA&rotenone@PAASH, abbreviated as MPER, by co-loading EDTA and rotenone in thiolated poly(acrylic acid) (PAASH)-modified mesoporous silica nanoparticles (MSNs), to concurrently chelate Mg^{2+} and stop Mg^{2+}-dependent glycolysis and disabling OXPHOS-mediated mitochondrial respiration for efficient tumor therapy without using any toxic chemodrug. Herein we named this strategy as "chemical suffocation therapy" (Scheme 1). MSNs were synthesized based on the Stöber mechanism, and afterwards, MSN@PAASH (MP) nanoparticles with excellent dispersity and monodispersed size were constructed by decorating polyvinyl pyrrolidone (PVP) and thiolated poly(acrylic acid) (PAASH) successively on the surface of MSNs according to a layer-by-layer strategy. PAASH serves as the gate keeper of MP nanoparticles, which will cleave and then release contents from the pore channels in response to the reducing tumor microenvironment (TME) once entrapped into tumors. Moreover, PAASH molecules will remain stable in the normal tissues preventing EDTA and rotenone from leaking into TME, guaranteeing the biosafety of MPER nanoparticles.

Due to the high-level GSH in the TME, after endocytosed into tumor cells, the PAASH shell of MPER nanoparticles will cleave into fragments due to the redox reaction with intracellular glutathione (GSH) and consequently release EDTA and rotenone from the pore channels into the cytoplasm. Mg^{2+}, one of the most abundant intracellular cations, is indispensable in the number of enzymes, especially those involved in the transfer of phosphate groups,[24] such as HK involved in the glucose phosphorylation, PFK involved in the fructose-6-phosphate dephosphorylation and PK involved in the phosphoenolpyruvate dephosphorylation, and all of these enzymes play important roles in the glycolytic process. As a strong chelator for Mg^{2+} (pK_a = 8.7) and Ca^{2+} (pK_a = 13.5),[12] EDTA molecules could chelate Mg^{2+} in the cytoplasm forming the EDTA–Mg complex and resultant glycolytic enzymes including HK, PFK and PK will be inactivated, which leads to glycolytic ATP generation inhibition. Though EDTA may prefer to chelate Ca^{2+} rather than Mg^{2+}, fortunately it has been found that Mg^{2+} can indeed be deprived by EDTA chelation thanks to its much higher concentration, which, therefore, results in largely inhibited ATP. Meanwhile, rotenone, a typical mitochondria inhibitor, diffuses into the intermembrane space of mitochondria and subsequently blocks the electron transfer by which O_2 could have been reduced to generate H_2O.

Accompanying the mitochondrial damage by rotenone, the OXPHOS and ATP generation processes taking place in mitochondria will be significantly inhibited. As a result, tumor cell

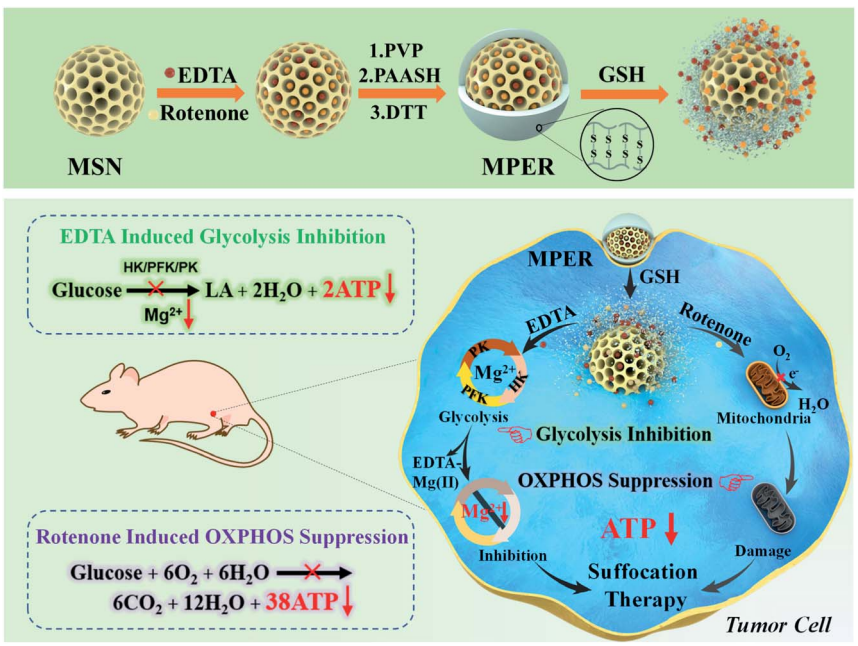

Scheme 1 Schematic illustration of the construction of an EDTA/rotenone co-loaded and GSH-responsive MSN nanoplatform by surface PVP and PAASH modifications, and the tumor chemical suffocation therapy strategy. The co-loaded EDTA and rotenone molecules inhibit glycolysis and aerobic respiration by chelating Mg^{2+} and blocking electronic transport during oxidative phosphorylation, respectively and simultaneously.

growth is largely suppressed by tumor cell suffocation *via* preventing both mitochondrial aerobic respiration and anoxic glycolysis. Importantly, the MSN surface-modified PAA shell and nanosized pore channels of MSNs themselves may enable the sustained releases of the loaded organic molecules for a long-term therapeutic efficacy. Additionally, it is worth noting that such a nanoplatform in response to a reductive TME would not be activated under the low GSH level conditions in the normal tissue, ensuring its successful tumor-specific therapy *in vivo*.

Results and discussions

Synthesis and characterization of MP nanoparticles

MSNs were chosen as the carrier for EDTA and rotenone deliveries thanks to its unique features, such as high surface area and volume pore, facile outer and inner surface modification, excellent biocompatibility, and so on.[25,26] MSN@PAASH (MP) nanoparticles with uniform spherical morphology and excellent water dispersity were synthesized by electrostatic interaction according to the literature,[27] followed by the layer-by-layer modification on the MSN surface with PVP and PAASH successively, and MP nanoparticles were finally prepared after the oxidation of PAASH molecules by strong reductant DTT to form –S–S– bonds in the surface-modified layer. Transmission electron microscopy (TEM) images show the uniform nanostructures of MSNs and MP nanoparticles of 47 and 54.5 nm in diameters from which the surface shell thickness of MP nanoparticles was determined to be about 7.5 nm (Fig. 1a and b).

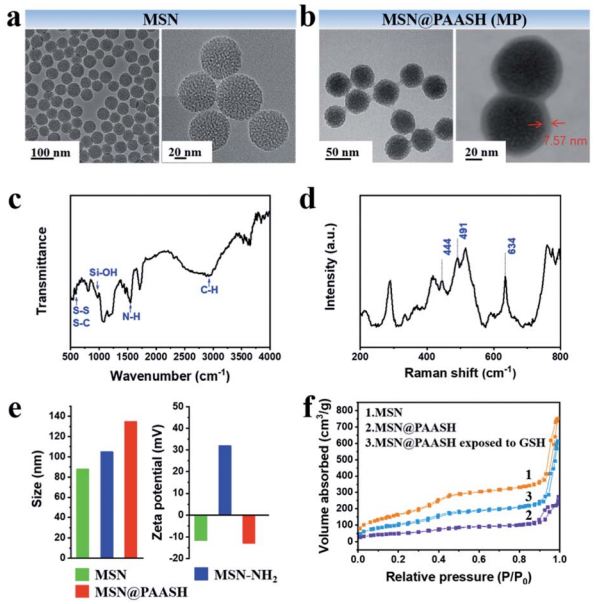

Fig. 1 Characterization of MSN@PAASH (MP) nanoparticles. TEM images of (a) MSN and (b) MSN@PAASH nanoparticles. (c) FTIR spectra and (d) Raman spectra of MSN@PAASH nanoparticles. (e) Particle-size distribution (left) and zeta potentials (right) of MSNs, MSN–NH_2 and MSN@PAASH nanoparticles. (f) Nitrogen adsorption–desorption isotherms of MSN (1), MSN@PAASH (2) and MSN@PAASH exposed to GSH (3).

The functional groups of PAASH shell and MP nanoparticles were then analyzed by Fourier-transform infrared (FTIR) spectra and Raman spectroscopy (Fig. 1c and d). The absorption peaks of Si–OH (960 cm^{-1}) and S–S, S–C bonds (520–720 cm^{-1})[28] can be found in Fig. 1c, indicating that the PAASH shell has been modified on the surface of MSNs. The thiol modification was performed *via* the amidation reaction between PAA and cysteine hydrochloride. Then, the –S–S– bond formed after the reduction of –SH by chloramine T. Raman spectroscopy is sensitive for detecting S–S bonds,[29] and S–S bond stretching vibrations can be clearly identified at 444 and 491 cm^{-1}, while the stretching mode of S–C bonds is at 634 cm^{-1}.[30,31] These findings confirm the successful S–S decoration of the MP nanoparticle shell. It is the presence of the PAASH shell that will ensure that loaded contents in MSN pore channels will not leak into the normal tissues, but will release within tumor cells.

The zeta potential and dynamic light scattering average diameter variations among MSN, MSN–NH_2 and MP nanoparticles indicate the success in each step of preparation (Fig. 1e). Because of the presence of abundant Si–OH groups on the spherical surface, the original MSNs were negative-charged (−11.7 mV). After the surface of MSNs was functionalized with amine groups by treatment with APTES, the zeta potential of obtained MSN–NH_2 turned positive (+32.0 mV). The surface charge of the final product MP nanoparticles was measured to be −13.0 mV, followed by PVP and PAASH modification through electrostatic adsorption. Furthermore, the DLS average diameters of the products during every step of decorating MSNs were determined to increase gradually from 85 nm to 135 nm, which were larger than those from TEM and SEM imaging (Fig. S1a and b†) to a different extent due to the existence of hydrated layers around the particle surface. Subsequently, the typical N_2 sorption isotherm technique was applied to measure the surface areas and pore volumes of MSNs and MP nanoparticles (Fig. 1f and S3a†). These results further indicate the successful shell assembly on the MSN surface according to which the dramatic surface area and pore volume decreases from 600.1 to 186.7 $m^2\ g^{-1}$ and from 0.92 to 0.34 mL g^{-1}, respectively, after the shell assembly (Fig. 1f and S3a†). Moreover, when exposed to 10 mM GSH for 48 h, the surface area and pore volume of MP nanoparticles recovered to 283.4 $m^2\ g^{-1}$ and 0.52 mL g^{-1}, respectively. These findings further confirm that MP nanoparticles possess a GSH-responsive core–shell structure.

Mg^{2+} depletion and glycolysis inhibition by MPE nanoparticles

There are totally ten successive steps in the pyruvate generation from glucose during the whole glycolytic process (Fig. 2a). Therein, enzymes including HK, PFK and PK will respectively and irreversibly catalyze the first, third and tenth reactions. Attractively, as an important common feature, the above-mentioned enzyme-catalyzed reactions which necessitate Mg^{2+} as a co-catalyst to catalyze reactions (Fig. S7a†). Based on such a common feature in the glycolysis, we propose to deliver EDTA to inactivate these rate-limiting enzymes by depleting Mg^{2+} *via* EDTA chelation in the cytoplasm (Fig. S7b†), consequently

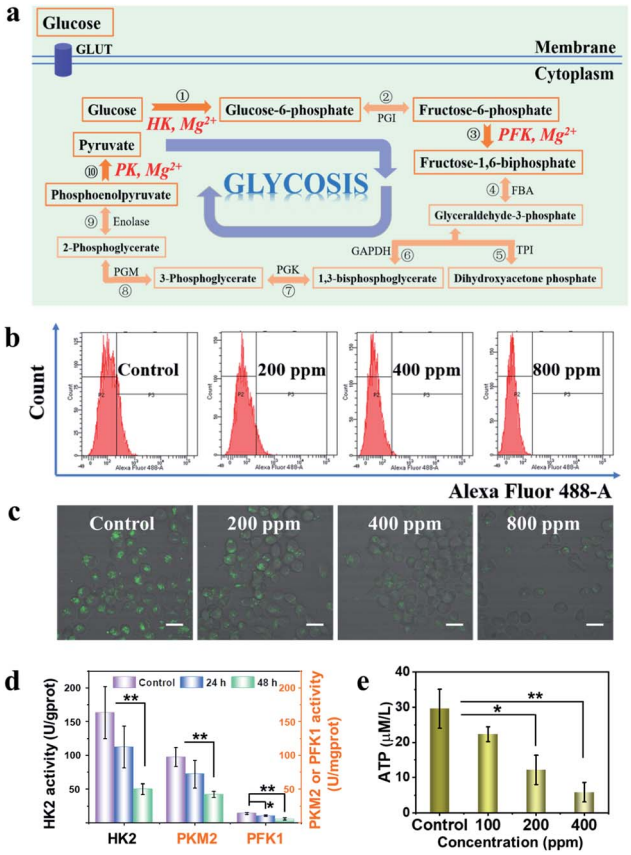

Fig. 2 Mg^{2+} depletion and glycolysis inhibition by MPE nanoparticles. (a) The schematic of the glycolytic process to produce pyruvate from glucose. (b) Flow cytometric fluorescence intensity analysis and (c) confocal fluorescence imaging (CLSM) of the intracellular Mg^{2+} of 4T1 cells stained with Mag-Fura-4 AM after incubation with varied concentrations of MPE for 24 h. Scale bar: 50 μm. (d) HK2, PKM2 and PFK1 activity variations after 4T1 cells being exposed to MPE nanoparticles (0 and 400 μg mL^{-1}) for 24 h and 48 h ($n = 4$). (e) ATP concentration after 4T1 cells being exposed to MPE nanoparticles for 24 h. All ATP measurements were based on 3 parallel experiments. *P < 0.05, **P < 0.01.

inhibiting the glycolytic process. Mag-Fura-4 AM with cell membrane permeability is sensitive to detect intracellular Mg^{2+}.[32] Therefore, the chelation effect of EDTA with intracellular Mg^{2+} of 4T1 cells stained with Mag-Fura-4 AM after incubation with EDTA-loaded MP (named as MPE) nanoparticles was investigated *via* flow cytometry and confocal laser scanning microscopy (CLSM). The fluorescence intensity of Mag-Fura-4 AM will increase significantly after binding with Mg^{2+} while free Mag-Fura-4 AM shows no fluorescence. The flow cytometric results (Fig. 2b) show that the fluorescence intensity of Mg-Mag-Fura-4 AM becomes largely decreased along with the prolonged incubation with varied concentrations of MPE nanoparticles, indicating that free Mg^{2+} in the cytoplasm has been mostly scavenged by EDTA chelation. In addition, the CLSM imaging (Fig. 2c) further confirms the results of flow cytometric analysis. The fluorescence signal becomes ever weaker at increased dosages of MPE nanoparticles. Moreover, the fluorescent intensity of Mg-Mag-Fura-4 AM in the HUVECs incubated with varied dosages of nanoparticles were also measured by flow cytometry (Fig. S9†). The fluorescent intensity shows little difference among various groups, which results from the protection of the disulfide-grafted PAA shell against the nanocarrier degradation, as well as the relatively low level GSH in HUVECs. This result evidences good biosafety of the nanoparticles. It can also be observed that, EDTA released from MSNs can chelate free Mg^{2+} effectively in the cytoplasm upon the cellular uptake of MPE nanoparticles in the tumour cells of the relatively high GSH concentration, in comparison to the less significant chelation of EDTA to Mg^{2+} by EDTA in the normal cells where the GSH concentration is much lower.

It is a common knowledge that EDTA will chelate Ca^{2+} more effectively than Mg^{2+}. To reveal any influence of Ca^{2+} chelation on Mg^{2+} depletion-related glycolytic enzyme activity, we investigated and found that MPE nanoparticles could indeed eliminate calcium in the cytoplasm, which, however, induces slight influence on the glycolytic enzymes (Fig. S8 and S9†). Flow cytometric fluorescence intensity analysis of the intracellular Ca^{2+} in 4T1 cells stained using a fluorescent probe Fluo-4 AM after incubation with varied concentrations of MPE for 24 h show that the calcium fluorescent intensity shows a remarkable fall in a MPE dosage-dependent manner (Fig. S8†). As Fluo-4 AM shows a specific combination with intracellular Ca^{2+}, we assessed the influence of such Ca^{2+} depletion on the Mg^{2+}-dependent glycolytic enzymes and ATP generation after 4T1 cells being incubated with Fluo-4 AM. The western blot results and the corresponding quantifications of HK2, PKM2 and PFK1 relative expressions in 4T1 cells incubated with Fluo-4 AM indicate that the HK2 and PKM2 expression remained almost unchanged compared with the untreated group, while PFK1 expression fell slightly (Fig. S10a and b†). Moreover, the ATP concentration of 4T1 cells shows a moderate decline after Fluo-4 AM incubation (Fig. S10c†). Taken together, the intracellular Ca^{2+} depletion by EDTA shows a less significant impact on the Mg^{2+}-dependent glycolytic process.

Furthermore, in order to understand the influence of intracellular Mg^{2+} deficiency on the rate-limiting glycolytic enzyme reactions by the chelation of EDTA released from MPE nanoparticles, we assessed the activities of intracellular HK2, PFK1 and PKM2 of 4T1 cells after incubation with MPE nanoparticles. As shown in Fig. 2d, after incubation for 48 h, the activities of HK2, PKM2 and PFK1 in 4T1 cells have respectively dropped from 166.6 U to 42.5 U per gram of protein, 98.9 U to 41.2 U per milligram of protein and from 13.9 U to 5.8 U per milligram of protein. These results indicate that the glycolytic enzyme activities have been inhibited markedly after magnesium ion chelation by EDTA. Subsequently, we investigated the influence of MPE nanoparticles at varied concentrations on the products of glycolysis, including lactic acid and ATP. After incubation with MPE nanoparticles for 24 h, the intracellular lactic acid concentration shows a negative correlation with the nanomaterial concentration (Fig. S11†). Moreover, the similar results of ATP level could be observed. Compared to the control group, the ATP production of 4T1 cells incubated with MPE nanoparticles for 24 h at 400 μg mL^{-1} has been substantially inhibited by 80.2% (Fig. 2e). Taken together, these results show

that the activities of rate-limiting glycolytic enzymes including HK2, PFK1 and PKM2 in 4T1 cells will reduce significantly after incubation with MPE nanoparticles due to the intracellular Mg^{2+} chelation by EDTA, consequently leading to the much diminished glycolytic products including lactic acid and ATP.

Cellular apoptosis and dual respiration inhibition mechanisms induced by MPER nanoparticles

We then introduced rotenone into MP nanoparticles and found that rotenone could destroy the mitochondrial structure and suppress OXPHOS of cancer cells by blocking the electron transport during the mitochondrial oxidative phosphorylation (Fig. S12 and S13†). Based on the above encouraging experimental results on effective glycolytic inhibition by EDTA released from MPE nanoparticles and OXPHOS suppression by rotenone released from MPR nanoparticles, next we co-loaded both EDTA and rotenone into MP nanoparticles, namely MPER nanoparticles, to inhibit both glycolysis and mitochondrial OXPHOS and simultaneously kill cancer cells. Subsequently, we investigated the intracellular therapeutic mechanism of MPER nanoparticles *via* flow cytometric analysis (Fig. S14†) after 4T1 cells being stained with a JC-1 probe. JC-1 monomers aggregate with each other to emit red fluorescence if mitochondrial membrane potential is normal, while it remains as monomers emitting green fluorescence if the mitochondrial membrane potential has collapsed. The control group (untreated 4T1 cells) and MP nanoparticles treated-4T1 cells emitted strong red fluorescence, manifesting that their mitochondrial membrane potentials are high enough. This result implies that MP nanoparticles as a drug carrier are bio-safe. Among MPE, MPR and MPER groups, MPER nanoparticle-treated 4T1 cells emitted the strongest green fluorescence, suggesting the highest level of mitochondrial membrane collapse.

Further, the cytotoxicity of MPER nanoparticles was investigated against human umbilical vein endothelial cells (HUVEC) *via* CCK-8 assays. As shown in Fig. 3a, the MPER nanoparticles show negligible effects on the HUVEC proliferation even when the concentration was elevated up to 800 μg mL^{-1} after incubation, showing low cytotoxicity to normal cells. Moreover, it has been demonstrated that MPR and MPE nanoparticles show moderate inhibition effect on 4T1 cell growth at concentrations up to 200 μg mL^{-1} after incubation. To our delight, when incubated with MPER nanoparticles, the relative cell viabilities of 4T1 cells exhibit a marked decline in a concentration-dependent manner with the suppression rate on relative cell viability being higher than 65% at the dose of 100 μg mL^{-1}. Besides, the MP nanoparticles show little toxicity to the 4T1 cells (Fig. S15†). These results indicate that MPER nanoparticles possess quite high therapeutic efficacy against the tumor cells, in comparison to the much lower efficacy of MP nanoparticles. Then the 4T1 cell apoptosis after incubation with MP, MPR, MPE and MPER nanoparticles was further verified by CLSM (Fig. 3b). After incubation for 24 h, the dead and live cells were differentiated by PI (red) and calcein-AM (green) co-staining, respectively. The CLSM pictures show that the MPER nanoparticle-incubated cells were mostly killed, demonstrating

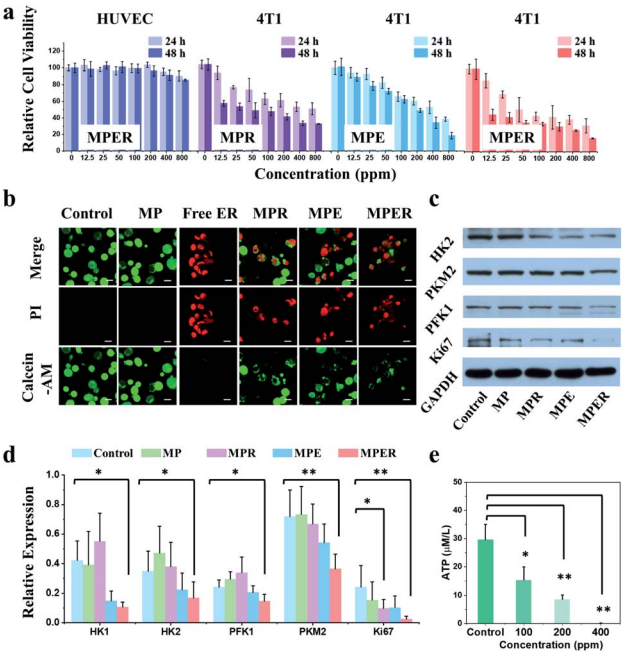

Fig. 3 Cellular apoptosis and dual respiration inhibition mechanisms induced by MPER nanoparticles. (a) Relative cell viabilities of HUVECs and 4T1 cells after being incubated with MPER nanoparticles. Every group of cytotoxicity measurements were performed on 6 parallel samples. (b) Confocal fluorescence images of calcein-AM and PI-stained 4T1 cells after various treatments. Herein, free ER refers to free EDTA and rotenone. Scale bar: 20 μm. (c) Western blot analyses of HK2, PFK1, PKM2 and Ki67 in 4T1 cells treated with MP, MPR, MPE and MPER nanoparticles. (d) The corresponding quantifications of HK2, PFK1, PKM2 and Ki67 relative expressions in 4T1 cells treated with MP, MPR, MPE and MPER nanoparticles. All western blot data were representative of 5 independent experiments. (e) ATP concentration of 4T1 cells after incubation with MPER nanoparticles. All ATP measurements were based on 3 parallel experiments. $*P < 0.05$, $**P < 0.01$.

the remarkable therapeutic effect of MPER nanoparticles *in vitro*. Moreover, it can be seen that MP nanoparticles show no toxicity to the cells while the free EDTA and rotenone show a strong tumor killing effect, suggesting that it is the released EDTA/rotenone from nanoparticles that kill tumor cells.

Glycolytic enzyme expressions after 4T1 cells incubated with MP, MPR, MPE and MPER nanoparticles were investigated by western blot analysis (Fig. 3c and d). Importantly, it has been found that MPR nanoparticles exhibit slight effect on these enzyme expressions, while MPE nanoparticles led to significant decline in glycolytic enzymes expression in 4T1 cells. Moreover, the MPER nanoparticles are stronger than that of MPE nanoparticles in inhibiting the expressions of the above glycolytic enzymes. Taken together, it can be concluded that the mitochondrial dysfunction induced by rotenone could strengthen the glycolytic inhibition effect by EDTA. Moreover, the down-regulation of Ki-67 by MPER nanoparticles demonstrates that the 4T1 cell proliferation has been significantly suppressed compared to the control group, in agreement with the above cell apoptosis results. Notably, when the concentration of MPER nanoparticles was elevated up to 400 μg mL^{-1}, the ATP level in 4T1 cells almost dropped to zero (Fig. 3e and Table S1†).

In vivo starvation therapy of MPER nanoparticles against tumors

Further, to verify the therapeutic efficacy of MPER *in vivo*, five groups of 4T1-bearing xenografts were treated with saline, MP, MPR, MPE and MPER nanoparticles. During a 14 day therapeutic period, the body weights of five groups presented neither abnormalities nor significant difference among each other (Fig. S16†). In 14 days, tumors of MP nanoparticles group kept growing quickly, indicating that MP nanoparticles possess no therapeutic effect *in vivo*. Comparatively, MPR and MPE nanoparticles showed moderate tumor inhibition effects compared to the control group (Fig. 4a). Importantly, according to the tumor volume and weight among each group at the endpoint of therapy, the tumor inhibition of MPER nanoparticles is most remarkable, showing the highest growth suppression rates of 66.8% and 73.7% in volume and weight (Fig. 4a, b and S17†), which are attributed to the combined dual-functional metabolic suppression roles of including the glycolytic inhibition and mitochondrial respiration destruction by the administrated MPER nanoparticles. In addition, at the endpoint in the tumor chemical suffocation therapy by MPER, the concentrations of HK2, PKM2 and PFK1 has decreased by 43.7%, 44.0% and 28.5%, respectively. The product of glucose metabolism, ATP, has declined by 38.4%. The results show that MPER nanoparticles could lead to the activity down regulation of these key glycolytic enzymes and energy supply suppression *in vivo* (Fig. 4c and d). In order to reveal the underlying therapeutic mechanisms by tumor-pathological analysis, Ki67 antibody and terminal deoxynucleotidyl transferase-mediated dUTP-biotin nick end labeling (TUNEL) staining of dissected tumor tissues between the control (saline) and MPER groups were conducted (Fig. 4e). As shown in the images of Ki67 staining in Fig. 4e, it could be directly observed that the cell proliferation in the experimental group has been significantly inhibited compared to the control group. Deoxynucleotidyl-mediated dUTP nick end labeling (TUNEL) staining and hematoxylin and eosin (H&E) staining images exhibit distinct apoptosis of tumor cells in the therapeutic group in comparison to the control group, demonstrating a significant therapeutic effect.

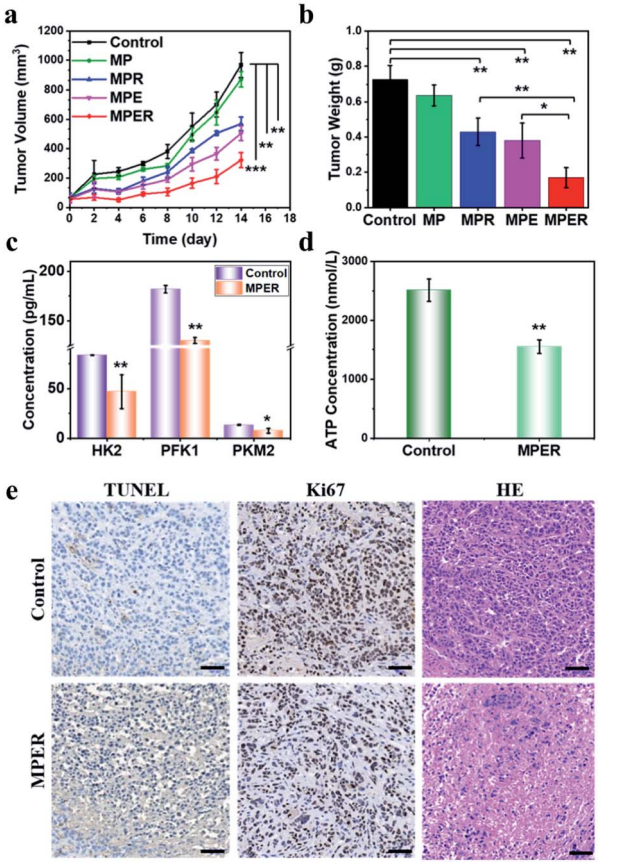

Fig. 4 *In vivo* starvation therapy of MPER nanoparticles against tumor. (a) Time-dependent tumor volume curves ($n = 5$, mean ± SD) after different treatments. All treatments were performed on day 0, 2 and 4 during the therapeutic period. (b) The tumor weights of dissected tumors from each group in 14 days. (c) HK2, PFK1, PKM2 and (d) ATP concentrations of tumor tissues after treatment with MPER nanoparticles at the concentrations of 25 and 0 mg kg^{-1} at the end of the therapy ($n = 4$). *$P < 0.05$, **$P < 0.01$, ***$P < 0.001$. (e) Ki67 immunohistochemical staining for cellular proliferation, TUNEL staining and hematoxylin–eosin staining (H&E) for pathological changes in tumor tissues from MPER and the control groups in 24 h of injection. Scale bar: 50 μm.

Conclusions

In summary, a GSH-responsive nanoplatform has been constructed for tumor suffocation therapy by concurrently suppressing both mitochondrial respiration and glycolysis *via* the co-deliveries of mitochondrial electron chain and glycolysis inhibitors. Surface-functionalized MSNs have been used to co-deliver EDTA as the Mg^{2+} chelator for glycolysis inhibition, and rotenone for mitochondrial respiration suppression to block both the glycolytic and aerobic respiration pathways of glucose metabolism, thus stopping the energy supply for maintaining cell growth. Especially, through releasing metal ion chelator EDTA when exposed to the high GSH level TME, the nanoplatform could deplete magnesium ions from cancer cells and consequently inactivate the corresponding enzymes necessary for glycolysis. Therein, the *in vivo* therapeutic performance of MPER nanoparticles exhibits effective tumor-inhibition efficacy toward 4T1 mammary tumor xenograft. This tumor suffocation therapeutic strategy not only reveals the effectiveness of glucose metabolism inhibition for tumor growth suppression, but also provides a promising tumor chemical therapeutic modality without using any highly toxic chemodrugs.

Author contributions

Professor Ph.D. Jianlin Shi and Ph.D. Ping Hu designed the idea of this work. Yingying Xu, Ph.D. Ping Hu and Professor Ph.D. Jianlin Shi designed the experiments, collecting the data and wrote this paper. All of the authors made contributions to the discussions during the whole work.

Conflicts of interest

There are no conflicts to declare.

Acknowledgements

All animal experiments in this study were performed in strict accordance with the guidelines by the Animal Care Ethics Commission of Tongji University School of Medicine (Accreditation number: SHDSYY-2018-Z0026), and the policies were approved by the Animal Care and Use Committee of Shanghai Tenth People's Hospital (Shanghai, China). This work was supported by National Natural Science Foundation of China (No. 21835007 and 52072394), Shanghai Science and Technology Committee Rising-Star Program (No. 19QA1410100), Shanghai International Cooperation Project (No. 20490714200), Key Research Program of Frontier Sciences, Chinese Academy of Sciences (No. ZDBS-LY-SLH029), and Youth Innovation Promotion Association of the Chinese Academy of Science (2019).

Notes and references

1 O. Warburg, *Science*, 1956, **123**, 309.
2 O. Warburg, K. Posener and E. Negelein, *Biochem. Z.*, 1924, **152**, 309.
3 V. B. Ritov and D. E. Kelley, *Diabetes*, 2001, **50**, 1253.
4 S. Kim, M. Cavalier, M. R. El-Maghrabi and Y. Lee, *J. Mol. Biol.*, 2007, **370**, 12.
5 S. Golshani-Hebroni, *Gene*, 2016, **581**, 1.
6 H. P. Morgan, F. J. O'Reilly, M. A. Wear, J. R. O'Neill, L. A. Fothergill-Gilmore, T. Hupp and M. D. Walkinshaw, *Proc. Natl. Acad. Sci. U. S. A.*, 2013, **110**, 5881.
7 R. Cabezas, M. F. Avila, J. Gonzalez, R. S. El-Bacha and G. E. Barreto, *Neurotoxic. Res.*, 2015, **27**, 355.
8 T. A. Sarafian, C. Montes, T. Imura, J. W. Qi, G. Coppola, D. H. Geschwind and M. V. Sofroniew, *PLoS One*, 2010, **5**, e9532.
9 Y. Kushnareva, A. N. Murphy and A. Andreyev, *Biochem. J.*, 2002, **368**, 545.
10 N. Y. Li, K. Ragheb, G. Lawler, J. Sturgist, B. Rajwa, J. A. Melendez and J. P. Robinson, *J. Biol. Chem.*, 2003, **278**, 8516.
11 T. H. Madden, A. K. Datye, M. Fulton, M. R. Prairie, S. A. Majumdar and B. M. Stange, *Environ. Sci. Technol.*, 1997, **31**, 3475.
12 S. Kolayli, M. Ocak, M. Kucuk and R. Abbasoglu, *Food Chem.*, 2004, **84**, 383.
13 D. Peer, J. M. Karp, S. Hong, O. C. FaroKhzad, R. Margalit and R. Langer, *Nat. Nanotechnol.*, 2007, **2**, 751.
14 S. Ganta, H. Devalapally, A. Shahiwala and M. Amiji, *J. Controlled Release*, 2008, **126**, 187.
15 S. Mura, J. Nicolas and P. Couvreur, *Nat. Mater.*, 2013, **12**, 991.
16 Q. Wang and D. O'Hare, *Chem. Rev.*, 2012, **112**, 4124.
17 A. Forterre, H. Komuro, S. Aminova and M. Harada, *Cancers*, 2020, **12**, 1852.
18 E. Bidram, Y. Esmaeili, H. Ranji-Burachaloo, N. Al-Zaubai, A. Zarrabi, A. Stewart and D. E. Dunstan, *J. Drug Delivery Sci. Technol.*, 2019, **54**, 101350.
19 D. Shao, M. Li, Z. Wang, X. Zheng, Y. Lao, Z. Chang, F. Zhang, M. Lu, J. Yue, H. Hu, H. Yan, L. Chen, W. Dong and K. W. Leong, *Adv. Mater.*, 2018, **30**, 1801198.
20 N. Song and Y. Yang, *Chem. Soc. Rev.*, 2015, **44**, 3474.
21 Y. Cui, H. Dong, X. Cai, D. Wang and Y. Li, *ACS Appl. Mater. Interfaces*, 2012, **4**, 3177.
22 Z. Luo, Y. Hu, K. Cai, X. Ding, Q. Zhang, M. Li, X. Ma, B. Zhang, Y. Zeng, P. Li, J. Li, J. Liu and Y. Zhao, *Biomaterials*, 2014, **35**, 7951.
23 O. Mezghrani, Y. Tang, X. Ke, Y. Chen, D. R. Hu, J. S. Tu, L. Zhao and N. Bourkaib, *Int. J. Pharm.*, 2015, **478**, 553.
24 P. W. Flatman, *Annu. Rev. Physiol.*, 1991, **53**, 259.
25 Y. Chen, H. Chen and J. Shi, *Expert Opin. Drug Delivery*, 2014, **11**, 917.
26 L. Pan, J. Liu, Q. He and J. Shi, *Adv. Mater.*, 2014, **26**, 6742.
27 Y. Liu, Y. Tian, Y. Tian, Y. Wang and W. Yang, *Adv. Mater.*, 2015, **27**, 7156.
28 L. Guo, J. Li, L. Zhang, J. Li, Y. Li, C. Yu, J. Shi, M. Ruan and J. Feng, *J. Mater. Chem.*, 2008, **18**, 2733.
29 C. Li, *J. Catal.*, 2003, **216**, 203.
30 J. Liu, Q. Yang, L. Zhang, D. Jiang, X. Shi, J. Yang, H. Zhong and C. Li, *Adv. Funct. Mater.*, 2007, **17**, 569.
31 L. Yu, Y. Chen, H. Lin, W. Du, H. Chen and J. Shi, *Biomaterials*, 2018, **161**, 292.
32 J. Zheng, Y. Kong, Y. Li and W. Zhang, *Stem Cell Res. Ther.*, 2019, **10**, 13.